

MicroRNA-132-mediated loss of p120RasGAP activates the endothelium to facilitate pathological angiogenesis

Sudarshan Anand¹, Bharat K Majeti¹, Lissette M Acevedo¹, Eric A Murphy¹, Rajesh Mukthavaram¹, Lea Schepke¹, Miller Huang¹, David J Shields¹, Jeffrey N Lindquist¹, Philip E Lapinski², Philip D King², Sara M Weis¹ & David A Cheresh¹

Although it is well established that tumors initiate an angiogenic switch, the molecular basis of this process remains incompletely understood. Here we show that the miRNA miR-132 acts as an angiogenic switch by targeting p120RasGAP in the endothelium and thereby inducing neovascularization. We identified miR-132 as a highly upregulated miRNA in a human embryonic stem cell model of vasculogenesis and found that miR-132 was highly expressed in the endothelium of human tumors and hemangiomas but was undetectable in normal endothelium. Ectopic expression of miR-132 in endothelial cells *in vitro* increased their proliferation and tube-forming capacity, whereas intraocular injection of an antagomir targeting miR-132, anti-miR-132, reduced postnatal retinal vascular development in mice. Among the top-ranking predicted targets of miR-132 was p120RasGAP, which we found to be expressed in normal but not tumor endothelium. Endothelial expression of miR-132 suppressed p120RasGAP expression and increased Ras activity, whereas a miRNA-resistant version of p120RasGAP reversed the vascular response induced by miR-132. Notably, administration of anti-miR-132 inhibited angiogenesis in wild-type mice but not in mice with an inducible deletion of *Rasa1* (encoding p120RasGAP). Finally, vessel-targeted nanoparticle delivery¹ of anti-miR-132 restored p120RasGAP expression in the tumor endothelium, suppressed angiogenesis and decreased tumor burden in an orthotopic xenograft mouse model of human breast carcinoma. We conclude that miR-132 acts as an angiogenic switch by suppressing endothelial p120RasGAP expression, leading to Ras activation and the induction of neovascularization, whereas the application of anti-miR-132 inhibits neovascularization by maintaining vessels in the resting state.

Endothelial cells in the adult mammal are among the least proliferative cell types, with about one in 10,000 cells entering the cell cycle at any given time². This quiescence is rapidly reversed in response to growth factors during pathological neovascularization, particularly during tumorigenesis³. The robust proliferative switch of the quiescent endothelium is a complex process that is governed by a network

of checks and balances. Small 22-nt RNAs called miRNAs are key regulators of several physiological processes, including angiogenesis⁴. To identify miRNAs that activate quiescent endothelium, we profiled miRNAs in both human umbilical vein endothelial cells (HUVECs) treated with the angiogenic growth factors vascular endothelial growth factor (VEGF) or basic fibroblast growth factor (bFGF) and in a human embryonic stem cell vasculogenesis model^{5,6} in which embryoid bodies derived from human embryonic stem cells form well defined endothelial networks after 14 d in culture (Supplementary Fig. 1). miR-132 had the highest combined rank of all miRNAs across these screens (Supplementary Fig. 2).

miR-132 is a highly conserved miRNA transcribed from an intergenic region on human chromosome 17 by the transcription factor cAMP response element binding protein (CREB)^{7,8}. Although no studies to our knowledge have linked miR-132 to endothelial cells, miR-132 can be expressed in neuronal cells upon stimulation with brain-derived neurotrophic factor (BDNF)⁸. Both VEGF and bFGF can rapidly induce CREB^{9,10}, but it is not known whether this activation is sustained enough to induce expression of miR-132 in endothelial cells. To address this issue, we investigated the kinetics of CREB phosphorylation in HUVECs and found that VEGF treatment induced peak activation of CREB after 15–30 min and, more notably, induced sustained activation for up to 9 h (Supplementary Fig. 3a). Accordingly, both VEGF and bFGF upregulated miR-132 in endothelial cells 3–6 h after treatment (Supplementary Fig. 3b). By contrast, miR-132 levels did not significantly change in human aortic smooth muscle cells treated with platelet-derived growth factor-BB (PDGF-BB; data not shown), indicating that miR-132's potential effects on neovascularization might primarily involve the endothelium.

As tumors are potent inducers of pathological neovascularization in adults, we investigated whether tumor-associated angiogenic factors can upregulate endothelial miR-132. Indeed, miR-132 was significantly upregulated in HUVECs treated with conditioned media from breast and pancreatic tumor cell lines (Supplementary Fig. 3c). In particular, conditioned medium from MDA-MB-231 human breast carcinoma cells promoted miR-132 expression to a similar degree as VEGF (Supplementary Fig. 3c). Treatment of HUVECs with MDA-MB-231-conditioned medium led to increased

¹Department of Pathology and Moores UCSD Cancer Center, University of California, San Diego, California, USA. ²Department of Microbiology and Immunology, University of Michigan, Ann Arbor, Michigan, USA. Correspondence should be addressed to D.A.C. (dcheresh@ucsd.edu).

Received 31 March; accepted 28 June; published online 1 August 2010; doi:10.1038/nm.2186

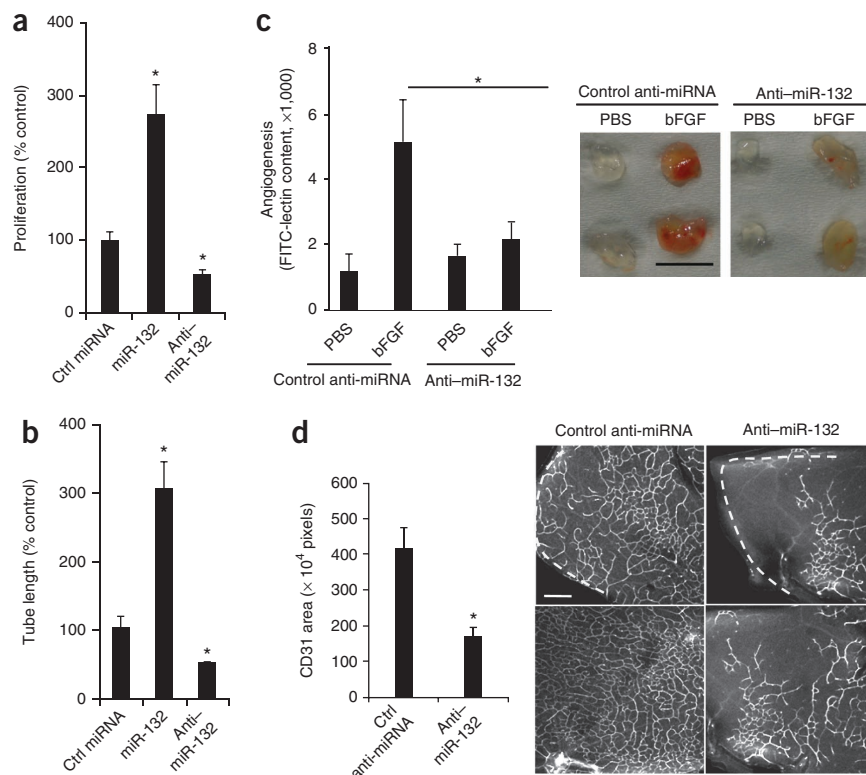
LETTERS

Figure 1 miR-132 regulates growth factor-mediated angiogenesis *in vitro* and *in vivo*.

(a) HUVEC cell proliferation. After transfection with miR-132 or anti-miR-132 or a control (Ctrl) miRNA, HUVECs were pulsed with BrdU and cell proliferation was measured using an ELISA assay. One representative experiment of three is shown, with the average values of triplicate wells. * $P < 0.01$ compared to control miRNA.

(b) HUVEC tube formation. 24 h after transfection as in a, HUVECs were suspended in a three-dimensional collagen matrix. Tube lengths were measured using MetaMorph software on day 4. One representative experiment of three is shown, with the average values of triplicate wells. * $P < 0.01$ compared to control miRNA.

(c) Angiogenesis in Matrigel plugs *in vivo*. Growth factor-reduced Matrigel containing either PBS or bFGF was injected subcutaneously into C57BL/6 mice. Mice received 10 μg of either a control anti-miRNA or anti-miR-132 in PBS intravenously ($n = 6$ per group). Angiogenesis was quantified by measuring FITC-lectin content on day 5. * $P < 0.05$ for control bFGF plugs compared to anti-miR-132 bFGF plugs. Right micrographs show representative Matrigel plugs from each group. Scale bar, 1 cm. (d) Retinal angiogenesis. Either control anti-miRNA or anti-miR-132 (1 μg) was injected intraocularly into 6-d-old BALB/c pups ($n = 5$ per group). Retinas were collected and stained with CD31-specific monoclonal antibodies (mAb). Bars show mean CD31 area ($n = 25$ fields) calculated using MetaMorph software. * $P < 0.01$. Right micrographs show representative confocal images of the deep plexus retinal vasculature. White dashed lines indicate the periphery of the retinas. Scale bar, 100 μm . Bars show means \pm s.e.m.



phosphorylation of CREB (indicating its activation) that was reversed by pretreatment with the VEGF receptor-2 (VEGFR-2) inhibitor vatalanib (Supplementary Fig. 3d). This result suggests that tumors could potentially upregulate endothelial miR-132 by activating CREB through a VEGFR-2-dependent pathway.

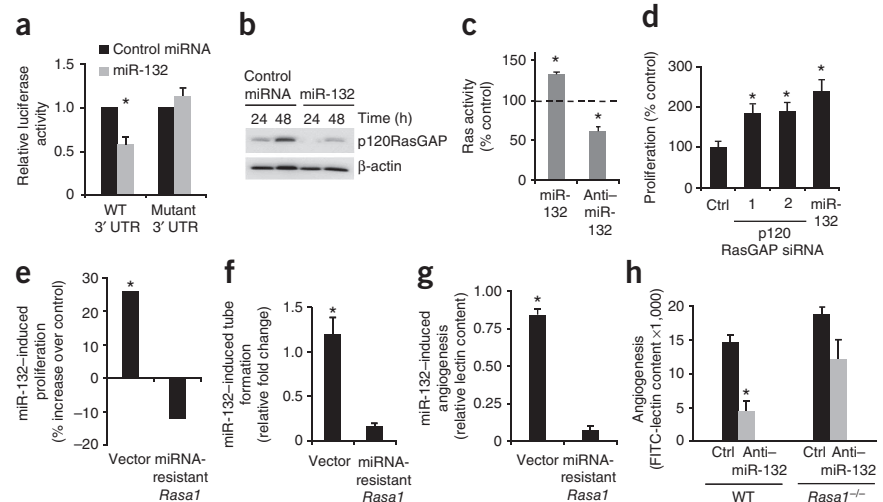
To investigate the effects of miR-132 on endothelial cells, we transfected HUVECs with mature human miR-132 or its complementary antagonist, anti-miR-132. We confirmed that these oligonucleotides were taken up by the cells (Supplementary Fig. 4a,b) and then tested their effects on cell proliferation *in vitro* and tube formation in a three-dimensional collagen matrix. miR-132 considerably increased cell proliferation and tube formation, whereas anti-miR-132 decreased these activities below baseline (Fig. 1a,b). Next, we investigated whether systemic administration of anti-miR-132 could inhibit angiogenesis *in vivo*. A single dose of anti-miR-132 significantly decreased bFGF-mediated angiogenesis in subcutaneous Matrigel implants in mice (Fig. 1c). This effect diminished over time and disappeared by day 8 (data not shown), indicating that sustained blockade of miR-132 might need a higher initial dose or continuous dosing with anti-miR-132. These data show that miR-132 can regulate growth factor-induced angiogenesis *in vitro* and *in vivo*.

Antiangiogenic agents that target the VEGFR pathway have shown considerable clinical benefit in patients with retinal diseases associated with pathological neovascularization^{11,12}. To assess the effects of miR-132 on retinal neovascularization, we treated 6-d-old mice undergoing postnatal retinal neovascularization with a single intraocular injection of anti-miR-132 and monitored vascular growth 6 d later. Anti-miR-132 produced a 50% decrease in retinal neovascularization in the deep plexus (Fig. 1d) but had no significant effect on

preestablished vessels in the superficial plexus (Supplementary Fig. 5a). Anti-miR-132 treatment did not alter perivascular coverage by smooth muscle cells in retinas (Supplementary Fig. 5b) or in established Matrigel plugs (data not shown), indicating that anti-miR-132 exerts its antiangiogenic effects by acting on endothelial cells rather than on perivascular cells. As our data show that miR-132 functions downstream of multiple angiogenic growth factors both *in vitro* in endothelial cells treated with VEGF and bFGF, and *in vivo* in bFGF Matrigel plugs, anti-miR-132 might produce a broader antivascular effect than agents that selectively target the VEGF pathway.

To identify the targets of miR-132 we used three algorithms, miRbase¹³, TargetScan¹⁴ and Pictar¹⁵, all of which predicted five potential direct targets (Supplementary Fig. 6a,b). RNAhybrid¹⁶ modeling of the 3' untranslated regions (UTRs) of these potential targets revealed that only the top candidate—*Rasa1*, encoding p120RasGAP (also known as RASA1 and RasGAP)—had more than one predicted miR-132 binding site in its 3' UTR. RNAhybrid modeling of the *Rasa1* 3' UTR predicted two miR-132 binding sites, separated by 40 bases (Supplementary Fig. 6c). The presence of such cooperative miRNA binding sites has been implicated in synergistic repression of targets¹⁷. Accordingly, ectopic expression of miR-132 suppressed a luciferase reporter upstream of a 70-bp region of the *Rasa1* 3' UTR (Fig. 2a). Mutagenesis of the seed sequences of the two predicted miR-132 binding sites restored luciferase expression, thereby confirming the specificity of the interaction between miR-132 and the *Rasa1* 3' UTR (Fig. 2a). Contact inhibition in endothelial cells led to upregulation of p120RasGAP expression after 48 h of growth in culture (Fig. 2b), consistent with the cell density-dependent increase in GAP activity reported in other cells¹⁸. Transfection of miR-132

Figure 2 Endothelial activation mediated by miR-132 depends on its downregulation of p120RasGAP. (a) Luciferase activity of 293T cells co-transfected with a luciferase-*Rasa1* 3' UTR plasmid containing either the WT 3' UTR or a mutated sequence, a β -galactosidase plasmid and either a control miRNA or miR-132. Bars shown mean relative luciferase activity normalized to the β -galactosidase levels ($n = 3$). * $P < 0.05$ compared to control miRNA. (b) Western blot detecting p120RasGAP in HUVECs transfected with either a control miRNA or miR-132. One representative experiment of two is shown. (c) Ras activity in HUVECs transfected with control miRNA, miR-132, control anti-miRNA or anti-miR-132. One representative experiment of two is shown, with the average value of triplicate wells. * $P < 0.05$ compared to control miRNA or control anti-miRNA. (d) HUVEC cell proliferation. After transfection with two different siRNAs (1 and 2) targeting p120RasGAP or with miR-132, HUVECs were pulsed with BrdU and cell proliferation was measured using an ELISA assay. Ctrl, control siRNA. One representative experiment of three is shown. * $P < 0.05$. Cell proliferation (e) and tube formation (f) of HUVECs. Cells were transfected with a control vector or a miRNA-resistant form of *Rasa1* and, 24 h later, were transfected with miR-132 or a control miRNA. The values shown are for miR-132 transfection relative to control miRNA transfection. One representative experiment of two is shown. * $P < 0.05$ (miR-132 compared with control miRNA). (g) Angiogenesis in Matrigel plugs *in vivo*. Forty-eight hours after mice were injected with bFGF Matrigel plugs, they were injected with either a control plasmid (vector) or a plasmid encoding miRNA-resistant *Rasa1* in nanoparticles. After a further 24 h, mice in each group ($n = 3$ per group) were treated with either a control miRNA or miR-132 in RGD nanoparticles. Angiogenesis in the plugs was quantified by measuring FITC-lectin content. The values shown are for mice receiving miR-132 normalized to those receiving control miRNA. One representative experiment of two is shown. * $P < 0.05$ (miR-132 compared with control miRNA). (h) Angiogenesis in Matrigel plugs *in vivo*. Tamoxifen-treated *Rasa1^{fl/fl} Ert2-ubiquitin-Cre* mice (*Rasa1^{-/-}*) ($n = 3$ per group) and wild-type mice ($n = 3$ per group) were injected with bFGF-containing Matrigel plugs and 2 h later treated with either a control anti-miRNA (Ctrl) or anti-miR-132. Angiogenesis was quantified by measuring FITC-lectin content. * $P < 0.05$ (anti-miR-132 compared with control anti-miRNA in WT mice). Bars show means \pm s.e.m.



into HUVECs decreased endogenous p120RasGAP expression by 70% in subconfluent cells (24 h of growth) and by 50% in confluent cells (48 h of growth; **Fig. 2b**) but did not affect any of the other targets predicted by all three algorithms, or known regulators of angiogenesis among the targets predicted by the *in silico* algorithms we used (**Supplementary Fig. 7**). Furthermore, knockdown of miR-132 with an anti-miR-132 markedly increased p120RasGAP levels *in vitro* in HUVECs (**Supplementary Fig. 8a**) and *in vivo* during bFGF-induced angiogenesis in subcutaneous Matrigel implants in mice (**Supplementary Fig. 8b,c**).

p120RasGAP is a known negative regulator of Ras that inactivates Ras by enhancing its intrinsic GTPase activity¹⁹. Accordingly, ectopic expression of miR-132 in HUVECs increased Ras activity, whereas anti-miR-132 reversed this effect, as measured in an ELISA assay using a GST-tagged, Ras-binding domain of Raf-1 to pull down active Ras (as detected with a Ras-specific antibody) (**Fig. 2c**). Consistent with its effects on Ras activity, anti-miR-132 substantially decreased VEGF-induced phosphorylation of mitogen-activated protein kinase extracellular related protein kinase kinase-1 (MEK-1) in HUVECs (**Supplementary Fig. 9**). Treatment of HUVECs with a MEK inhibitor (PD0325901) abrogated the proliferative effects of miR-132 (**Supplementary Fig. 9**). Moreover, knockdown of p120RasGAP using either of two different siRNAs increased endothelial proliferation to a similar extent as did miR-132 (**Fig. 2d**). Notably, expression of a miR-resistant *Rasa1* lacking its 3' UTR was sufficient to abrogate the miR-132-induced increase in cell proliferation (**Fig. 2e**) and tube formation (**Fig. 2f**) *in vitro* as well as angiogenesis in bFGF-containing Matrigel plugs *in vivo* (**Fig. 2g**).

To further elucidate the role of p120RasGAP in mediating miR-132's effects, we crossed mice containing *loxP*-flanked (floxed) alleles of *Rasa1* with *Ert2-ubiquitin-Cre* mice²⁰ to generate mice in

which *Rasa1* can be deleted by tamoxifen administration. Tamoxifen binding to the estrogen receptor Ert2 leads to expression of the Cre recombinase gene downstream of the ubiquitin promoter, resulting in a deletion of the floxed allele in all cell types. Injection of tamoxifen into these mice led to a substantial decrease in p120RasGAP expression in multiple tissues (data not shown). Treatment of these mice, which lacked p120RasGAP, with anti-miR-132 did not markedly decrease angiogenesis in Matrigel plugs, as it did in control mice (**Fig. 2h**). Thus, the functional consequences of miR-132 in endothelial cells are predominantly, if not exclusively, mediated through its regulation of p120RasGAP expression. Moreover, we found that miR-132 could promote cell proliferation through downregulation of p120RasGAP in the mouse endothelioma cell line b.End3 (**Supplementary Fig. 10**), indicating that this regulatory circuit might act as a conserved angiogenic switch mechanism regulating endothelial survival, growth or both.

Previous studies have provided evidence that p120RasGAP acts as a crucial negative regulator of vascular development and remodeling. For instance, deletion of *Rasa1* causes severe vascular remodeling and embryonic lethality in mice²¹. Mutations in the human gene encoding p120RasGAP have been linked to capillary and arteriovenous malformations and Parkes-Weber syndrome²²⁻²⁴. On the basis of these observations, we hypothesized that during tumor neovascularization, miR-132 levels would increase in angiogenic endothelial cells, thereby reducing p120RasGAP expression. Indeed, endothelial cells in human breast tumors had abundant levels of miR-132 and minimal amounts of p120RasGAP (**Fig. 3a,b**). By contrast, the endothelium of normal human breast tissue expressed abundant p120RasGAP but contained no detectable miR-132, as measured by *in situ* hybridization (**Fig. 3a,b**). This reciprocal expression of p120RasGAP and miR-132 was not unique to breast carcinoma but was also seen in

LETTERS

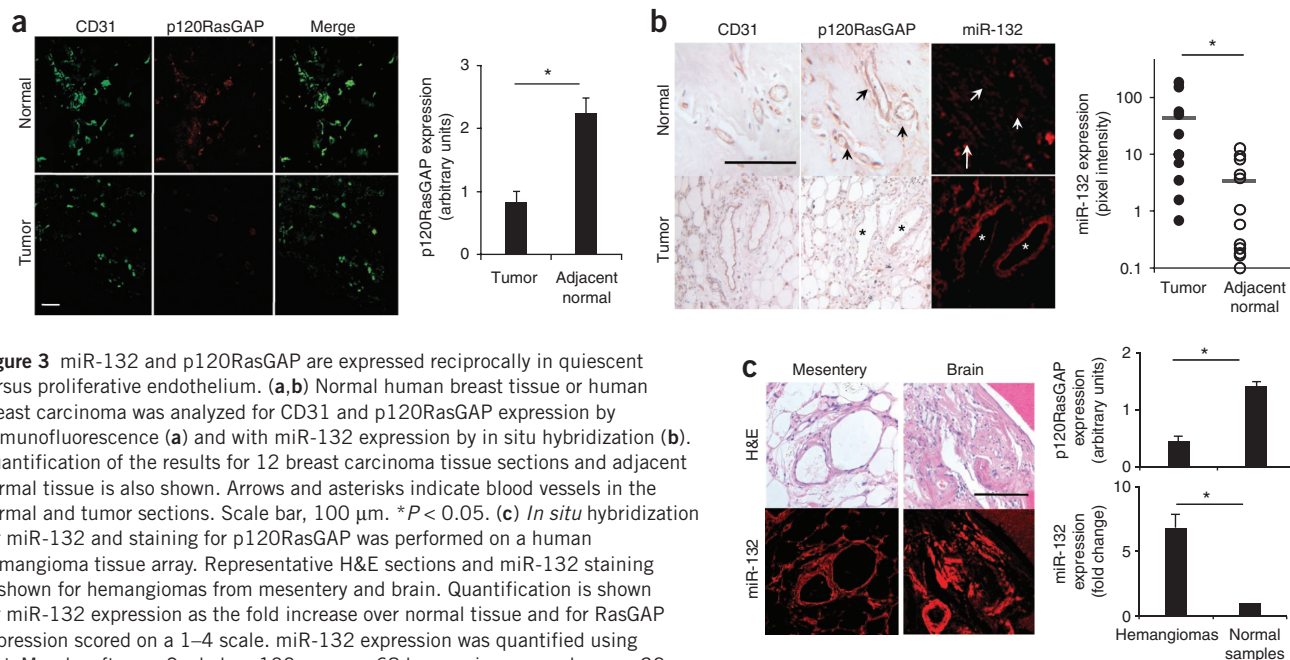


Figure 3 miR-132 and p120RasGAP are expressed reciprocally in quiescent versus proliferative endothelium. (a,b) Normal human breast tissue or human breast carcinoma was analyzed for CD31 and p120RasGAP expression by immunofluorescence (a) and with miR-132 expression by in situ hybridization (b). Quantification of the results for 12 breast carcinoma tissue sections and adjacent normal tissue is also shown. Arrows and asterisks indicate blood vessels in the normal and tumor sections. Scale bar, 100 μ m. * P < 0.05. (c) *In situ* hybridization for miR-132 and staining for p120RasGAP was performed on a human hemangioma tissue array. Representative H&E sections and miR-132 staining is shown for hemangiomas from mesentery and brain. Quantification is shown for miR-132 expression as the fold increase over normal tissue and for RasGAP expression scored on a 1–4 scale. miR-132 expression was quantified using MetaMorph software. Scale bar, 100 μ m. n = 68 hemangioma samples; n = 32 normal samples. * P < 0.05, Mann-Whitney U test. Bars show means \pm s.e.m.

the endothelium of orthotopic murine pancreatic tumors relative to normal mouse pancreas (Supplementary Fig. 11). In these breast tumors, p120RasGAP was readily detectable on perivascular structures associated with the tumor neovasculature (data not shown). Moreover, 75% of human hemangiomas tested (51/68) expressed miR-132 but had no detectable expression of p120RasGAP, confirming that miR-132 is a marker of hyperproliferative or activated endothelium (Fig. 3c and Supplementary Fig. 12). The reciprocal expression of miR-132 in proliferative endothelium and p120RasGAP in quiescent endothelium suggests that the regulation of p120RasGAP by miR-132 can facilitate an angiogenic switch. Our observation that PDGF-BB, a growth factor for smooth muscle and stromal cells, does not upregulate miR-132 in human aortic smooth muscle cells *in vitro* suggests that the miR-132–p120RasGAP regulatory mechanism is specific for the endothelium.

On the basis of these observations, we hypothesized that inhibition of miR-132 in the tumor vasculature might result in decreased angiogenesis and tumor burden by restoring the expression of p120RasGAP. To test this hypothesis, we used an integrin $\alpha_v\beta_3$ -targeted nanoparticle that can deliver nucleic acids²⁵ or drugs¹ to the tumor neovasculature for selective delivery of anti-miR-132 to the tumor endothelium of mice. We confirmed that these nanoparticles were able to deliver a fluorescently labeled anti-miR-132 to tumor vasculature (Supplementary Fig. 13). Systemic administration of anti-miR-132 nanoparticles not only blocked angiogenesis induced by a VEGF-secreting ovarian carcinoma in mice (Supplementary Fig. 14) but also significantly decreased tumor burden and angiogenesis in an orthotopic xenograft mouse model of human breast carcinoma, MDA-MB 231 (Fig. 4a,b and Supplementary Fig. 14). After treatment with anti-miR-132 nanoparticles, the vasculature of these mice showed increased endothelial p120RasGAP (Fig. 4c,d), thereby confirming that antagonism of miR-132 can restore p120RasGAP expression during neovascularization *in vivo*. Although anti-miR-132 treatment did not affect the expression p120RasGAP in myeloid cells, tumor cells or stromal cells (data not shown), we did observe a twofold increase

in p120RasGAP in lymphatic endothelial cells identified by positive staining for lymphatic vessel endothelial hyaluronan receptor (LYVE-1; Supplementary Fig. 15). However, unlike the CD31⁺ endothelial area, which was reduced upon anti-miR-132 treatment (Fig. 4b), the area of LYVE-1⁺ cells was not markedly different between the groups (data not shown), suggesting that anti-miR-132 does not affect lymphangiogenesis in these tumors. Moreover, anti-miR-132 did not affect the proliferation of the MDA-MB-231 cells *in vitro* and had no effect on perivascular cells as measured by the area of smooth muscle actin staining colocalizing with CD31 in the MDA-MB-231 tumors (data not shown).

Angiogenesis is a complex process that depends on the balance of pro- and antiangiogenic factors that influence the quiescence or proliferative state of the endothelium in a wide variety of disease states. We show here that miR-132 is expressed in activated endothelial cells, where it suppresses p120RasGAP expression, permitting activation of Ras and leading to neovascularization. Moreover, neutralization of miR-132 with an antagomir suppresses retinal and tumor angiogenesis, pointing toward a new therapeutic strategy for diseases associated with pathological angiogenesis. miR-126 has recently been described to affect developmental neovascularization by targeting several well known angiogenic pathways and transcription factors such as Sprouty-related EVH-1 domain containing-1 (SPRED-1)^{26–28}, but the role of miR-126 in pathological angiogenesis has yet to be determined.

Other miRNAs, notably miR-296 (ref. 29) and miR-92a (ref. 30), have been described as positive or negative regulators of angiogenesis. miR-296 was identified in a screen for endothelial miRNAs that were dysregulated during co-culture with a human glioma cell line and miR-296 was shown to target HGS (hepatocyte growth factor-regulated tyrosine kinase substrate), an endosome-associated protein that affects sorting and trafficking of growth factor receptors³¹. Although blockade of miR-296 decreases angiogenesis in tumor xenografts²⁹, it is unclear whether such blockade produces a substantial decrease in tumor burden *in vivo*. In our screens, miR-296 was upregulated in

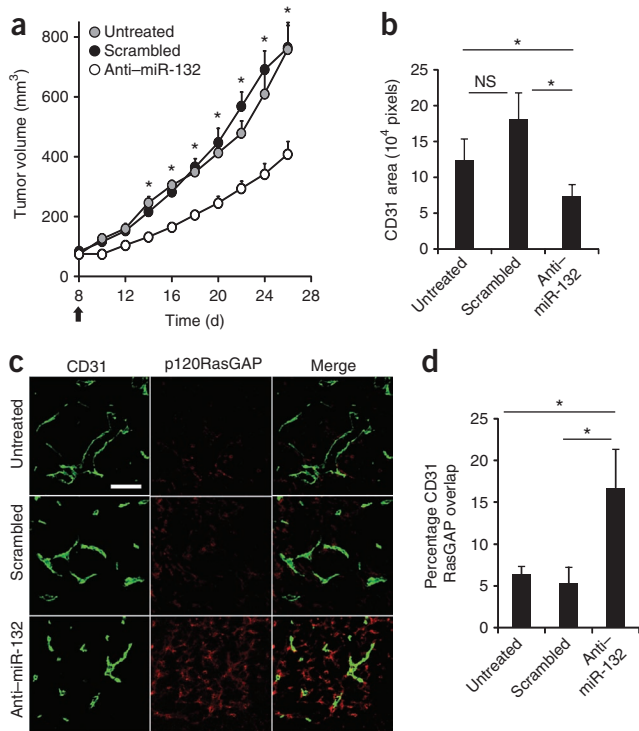


Figure 4 Targeted delivery of anti-miR-132 decreases tumor burden by restoring endothelial p120RasGAP. Nude mice were implanted with 2×10^6 MDA-MB 231 cells in the mammary fat pad. The tumors were measured 8 d later, and mice with palpable tumors of similar volumes were randomly assigned to three groups. Mice were left untreated or received 50 μ g of scrambled anti-miRNA or anti-miR-132 every 48 h until day 24. (a) Tumor volumes (mean \pm s.e.m) of at least seven mice per group, starting from the day of treatment (black arrow). * $P < 0.05$ compared to anti-miR-132. (b–d) Immunofluorescent staining of CD31 and p120RasGAP in tumor sections from at least three mice per group. (b) Microvessel density measured by CD31 area. (c) Representative images of p120RasGAP expression in CD31-positive cells. Scale bar, 100 μ m. (d) Quantification of the overlap of CD31 and p120RasGAP expression (percentage of CD31 cells that are also positive for RasGAP expression). Pixel density was quantified using MetaMorph software. Bars are mean \pm s.e.m of multiple images from at least three mice per group. * $P < 0.05$ (anti-miR-132 compared to untreated or scrambled). NS, not significant.

growth factor-treated endothelial cells but not in the developmental angiogenesis screen using human embryonic stem cells. By contrast, miR-132 was upregulated in endothelial activation during both developmental and pathological neovascularization. Although these two models have different kinetics and growth factor requirements and recapitulate distinct physiological responses, they share common features: activation of the proliferation, migration and tube formation programs of endothelial cells. Accordingly, anti-miR-132 blocked not only growth factor-induced angiogenesis *in vitro* and *in vivo* but also developmental angiogenesis in neonatal retinas, highlighting the conserved nature of this angiogenic switch mechanism.

Although p120RasGAP has been reported to have Ras-dependent and Ras-independent functions³², growth factor-mediated activation of Ras is sufficient to induce a proangiogenic phenotype in primary endothelial cells³³. In fact, the loss of p120RasGAP alone was sufficient to mediate an enhanced angiogenic response to bFGF in Matrigel plugs (Supplementary Fig. 16). Suppression of p120RasGAP expression seems to be crucial in facilitating angiogenesis *in vivo*,

because anti-miR-132 can both restore p120RasGAP expression and decrease neovascularization in several tumor models. On the basis of these observations, we believe it is likely that miR-132 can regulate various endothelial cell activities, including proliferation, survival, migration and tube formation, to exert its effects on angiogenesis.

There is emerging evidence that some of the current antiangiogenic therapies, which target single pathways such as the VEGFR pathway, can lead to the development of 'evasive resistance' in tumors through the upregulation of alternative growth factors³⁴. In this context, antagonism of endogenous regulators such as miR-132 that are induced under pathological conditions and target 'gatekeepers' of endothelial activation such as p120RasGAP may represent a powerful strategy to inhibit angiogenesis in a wide range of pathological conditions. To our knowledge, the findings reported here provide the first description of a miRNA-regulated angiogenic switch. Our studies show that this switch can be regulated to both disrupt and facilitate neovascularization. The possibility of delivering miRNAs or antagomirs to activated endothelium, as demonstrated here using miR-132-containing nanoparticles targeted to integrin $\alpha_V\beta_3$, suggests opportunities for manipulating miRNA levels in the endothelium to control pathological neovascularization.

METHODS

Methods and any associated references are available in the online version of the paper at <http://www.nature.com/naturemedicine/>.

Note: Supplementary information is available on the Nature Medicine website.

ACKNOWLEDGMENTS

We thank L. Barnes, E. Goka, B. Walsh and D. Wu for technical support. We thank S. Weng and J. Desgrosellier for discussions. We thank E. Brown (University of Pennsylvania) for the *Ert2*-ubiquitin-Cre mice. We thank R. Kerbel (University of Toronto) for the fast-growing variant of MDA-MB-231 breast carcinoma cells. We thank S. Kajiji (Scripps Research Institute) for FG human pancreatic adenocarcinoma cells. This work was supported by US National Institutes of Health grants HL078912, CA104898 and CA050286 to D.A.C. and HL096498 to P.D.K. S.A. is supported in part by an American Heart Association postdoctoral fellowship 09POST2040038.

AUTHOR CONTRIBUTIONS

S.A. and D.A.C. designed the study. E.A.M., B.K.M. and R.M. designed the nanoparticles. J.N.L. established the human ES cell vasculogenesis model. D.J.S. helped with the TaqMan microRNA panel experiments and analysis. P.E.L. and P.D.K. generated and characterized the *Rasa1*^{fl/fl} mice. S.A., L.S., L.M.A. and M.H. performed experiments and analyzed data. S.A., S.M.W. and D.A.C. analyzed data and wrote the manuscript. D.A.C. supervised the project.

COMPETING FINANCIAL INTERESTS

The authors declare no competing financial interests.

Published online at <http://www.nature.com/naturemedicine/>.

Reprints and permissions information is available online at <http://npg.nature.com/reprintsandpermissions/>.

- Murphy, E.A. *et al.* Nanoparticle-mediated drug delivery to tumor vasculature suppresses metastasis. *Proc. Natl. Acad. Sci. USA* **105**, 9343–9348 (2008).
- Hobson, B. & Denekamp, J. Endothelial proliferation in tumours and normal tissues: continuous labelling studies. *Br. J. Cancer* **49**, 405–413 (1984).
- Folkman, J. The role of angiogenesis in tumor growth. *Semin. Cancer Biol.* **3**, 65–71 (1992).
- Fish, J.E. & Srivastava, D. MicroRNAs: opening a new vein in angiogenesis research. *Sci. Signal.* **2**, pe1 (2009).
- Lindquist, J.N., Cheresh, D.A. & Snyder, E.Y. Derivation of vasculature from embryonic stem cells. *Curr. Protoc. Stem Cell Biol.* **12**, 1.1F.9.1–1.1F.9.6 (2010).
- Kelly, M.A. & Hirschi, K.K. Signaling hierarchy regulating human endothelial cell development. *Arterioscler. Thromb. Vasc. Biol.* **29**, 718–724 (2009).
- Nudelman, A.S. *et al.* Neuronal activity rapidly induces transcription of the CREB-regulated microRNA-132, *in vivo*. *Hippocampus* **20**, 492–498 (2010).
- Vo, N. *et al.* A cAMP-response element binding protein-induced microRNA regulates neuronal morphogenesis. *Proc. Natl. Acad. Sci. USA* **102**, 16426–16431 (2005).

LETTERS

9. Mayo, L.D., Kessler, K.M., Pincheira, R., Warren, R.S. & Donner, D.B. Vascular endothelial cell growth factor activates CRE-binding protein by signaling through the KDR receptor tyrosine kinase. *J. Biol. Chem.* **276**, 25184–25189 (2001).
10. Tan, Y. *et al.* FGF and stress regulate CREB and ATF-1 via a pathway involving p38 MAP kinase and MAPKAP kinase-2. *EMBO J.* **15**, 4629–4642 (1996).
11. Kenneth, T.E. & Kertes, P.J. Ranibizumab in neovascular age-related macular degeneration. *Clin. Interv. Aging* **1**, 451–466 (2006).
12. Gragoudas, E.S., Adamis, A.P., Cunningham, E.T. Jr., Feinsod, M. & Guyer, D.R. Pegaptanib for neovascular age-related macular degeneration. *N. Engl. J. Med.* **351**, 2805–2816 (2004).
13. Griffiths-Jones, S., Grocock, R.J., van Dongen, S., Bateman, A. & Enright, A.J. miRBase: microRNA sequences, targets and gene nomenclature. *Nucleic Acids Res.* **34**, D140–D144 (2006).
14. Lewis, B.P., Burge, C.B. & Bartel, D.P. Conserved seed pairing, often flanked by adenosines, indicates that thousands of human genes are microRNA targets. *Cell* **120**, 15–20 (2005).
15. Krek, A. *et al.* Combinatorial microRNA target predictions. *Nat. Genet.* **37**, 495–500 (2005).
16. Rehmsmeier, M., Steffen, P., Hochsmann, M. & Giegerich, R. Fast and effective prediction of microRNA/target duplexes. *RNA* **10**, 1507–1517 (2004).
17. Bartel, D.P. MicroRNAs: target recognition and regulatory functions. *Cell* **136**, 215–233 (2009).
18. Hoshino, M., Kawakita, M. & Hattori, S. Characterization of a factor that stimulates hydrolysis of GTP bound to ras gene product p21 (GTPase-activating protein) and correlation of its activity to cell density. *Mol. Cell. Biol.* **8**, 4169–4173 (1988).
19. McCormick, F. ras GTPase activating protein: signal transmitter and signal terminator. *Cell* **56**, 5–8 (1989).
20. Lapinski, P.E. *et al.* Generation of mice with a conditional allele of the p120 Ras GTPase-activating protein. *Genesis* **45**, 762–767 (2007).
21. Henkemeyer, M. *et al.* Vascular system defects and neuronal apoptosis in mice lacking ras GTPase-activating protein. *Nature* **377**, 695–701 (1995).
22. Boon, L.M., Mulliken, J.B. & Viskula, M. RASA1: variable phenotype with capillary and arteriovenous malformations. *Curr. Opin. Genet. Dev.* **15**, 265–269 (2005).
23. Eerola, I. *et al.* Capillary malformation-arteriovenous malformation, a new clinical and genetic disorder caused by RASA1 mutations. *Am. J. Hum. Genet.* **73**, 1240–1249 (2003).
24. Hershkovitz, D., Bercovich, D., Sprecher, E. & Lapidot, M. RASA1 mutations may cause hereditary capillary malformations without arteriovenous malformations. *Br. J. Dermatol.* **158**, 1035–1040 (2008).
25. Hood, J.D. *et al.* Tumor regression by targeted gene delivery to the neovasculature. *Science* **296**, 2404–2407 (2002).
26. Fish, J.E. *et al.* miR-126 regulates angiogenic signaling and vascular integrity. *Dev. Cell* **15**, 272–284 (2008).
27. Harris, T.A., Yamakuchi, M., Ferlito, M., Mendell, J.T. & Lowenstein, C.J. MicroRNA-126 regulates endothelial expression of vascular cell adhesion molecule 1. *Proc. Natl. Acad. Sci. USA* **105**, 1516–1521 (2008).
28. Wang, S. *et al.* The endothelial-specific microRNA miR-126 governs vascular integrity and angiogenesis. *Dev. Cell* **15**, 261–271 (2008).
29. Würdinger, T. *et al.* miR-296 regulates growth factor receptor overexpression in angiogenic endothelial cells. *Cancer Cell* **14**, 382–393 (2008).
30. Bonauer, A. *et al.* MicroRNA-92a controls angiogenesis and functional recovery of ischemic tissues in mice. *Science* **324**, 1710–1713 (2009).
31. Komada, M. & Kitamura, N. The Hrs/STAM complex in the downregulation of receptor tyrosine kinases. *J. Biochem.* **137**, 1–8 (2005).
32. Kulkarni, S.V., Gish, G., van der Geer, P., Henkemeyer, M. & Pawson, T. Role of p120 Ras-GAP in directed cell movement. *J. Cell Biol.* **149**, 457–470 (2000).
33. Meadows, K.N., Bryant, P., Vincent, P.A. & Pumiglia, K.M. Activated Ras induces a proangiogenic phenotype in primary endothelial cells. *Oncogene* **23**, 192–200 (2004).
34. Bergers, G. & Hanahan, D. Modes of resistance to anti-angiogenic therapy. *Nat. Rev. Cancer* **8**, 592–603 (2008).

ONLINE METHODS

Cell culture and reagents. HUVECs (Lonza) were cultured in EBM-2 media (Lonza) supplemented with bullet kit containing various growth factors (Lonza) and 10% FCS (Hyclone). bEnd.3 cells were obtained from American Type Culture Collection and cultured in complete DMEM. For starvation experiments, serum-free and growth factor-free medium was used. MDA-MB-231Lm2-4 Luc⁺ cells, a fast-growing variant of human breast carcinoma cells³⁵, were a gift from R. Kerbel (University of Toronto). FG human pancreatic adenocarcinoma cells were a gift from S. Kajiji (Scripps Research Institute) and are described elsewhere⁴⁰. R40P mouse pancreatic carcinoma cells were derived from a primary tumor in a pancreas-specific *Ink4a*-deficient, oncogenic K-Ras G12D-expressing mouse¹, and RCP30 cells were derived from a primary tumor in a pancreas-specific *Csk*-deficient, oncogenic K-Ras G12D-expressing mouse (D.J.S. and D.A.C., unpublished observations). WA09 (H9) human embryonic stem cells were cultured in KO-DMEM (Gibco) supplemented with 15% Knockout (KO) Serum Replacement (SR) (Gibco) and 20 ng ml⁻¹ bFGF (Chemicon) on gamma-irradiated hs27 human fibroblast cells (American Type Culture Collection). Undifferentiated human embryonic stem cell colonies were manually dissected and allowed to form embryoid bodies in suspension for 5–7 d in KO-DMEM with 15% KO-SR. Embryoid bodies were seeded onto collagen-coated dishes and allowed to differentiate. Cultures were grown in DMEM supplemented with N2 supplement (Invitrogen), 20 ng ml⁻¹ bFGF (Chemicon) and 25 ng ml⁻¹ VEGF (Peprotech). Fresh medium was added every other day for up to 28 d.

Antibodies to p120RasGAP (SC-63), angiominin (SC-82491), SMAD5 (SC-26418), TMEFF1 (SC-98956), SIRT1 (SC-15404) were from Santa Cruz Biotechnology. Antibodies to mouse CD31 (550274), human CD31 (550389), VE cadherin (555661) and GCF2 (also known as LRRFIP1) (612161) were from BD Biosciences. β -actin-specific antibody (A5316) was from Sigma. Antibodies to CREB (9104) and p-CREB (9191) were from Cell Signaling. siRNAs targeting p120RasGAP were from Qiagen. The MEK inhibitor PD0325901 was from Chemietek.

Vectors and plasmids. The mutant *Rasa1* 3' UTR was generated by replacing both copies of the miR-132 seed sequence GACTGTT with TGTCAGG in a ~70-bp fragment of the wild type 3' UTR as shown below (the seed sequence is underlined) and by ligation into the pmir-REPORT vector (Ambion).

Wild-type 3' UTR: 5'-TGTGTATAACTGGATTGCAGACTGTTCTTACTGTA
TAACTACTTCCTGATTAGGAATATGACCATTGACTGTTC-3'

Mutant UTR: 5'-TGTGTATAACTGGATTGCATGTCAGGCTTACTGTAA
CTACTTCCTGATTAGGAATATGACCATTGTCAGG-3'

The miR-resistant *Rasa1* construct was generated by cloning the *Rasa1* cDNA from the start codon until the stop codon, thereby excluding the 3' UTR region, into the pCDH vector backbone (CD511-B1 from System Biosciences). An empty backbone vector was used as a control.

MicroRNAs and anti-microRNAs. Control miRNA, control anti-miRNA, miR-132 and anti-miR-132 were from Ambion: miR-132, 5'-UAACAGUCUACAG CCAUGGUCG-3'; Anti-miR-132: 5'-CGACCATGGCTGTAGACTGTTA-3'. For *in vivo* studies that involved large doses of anti-miRNA treatments, oligomers with the same sequence were synthesized on a larger scale from Sigma.

Scrambled anti-miRNA: 5'-[mA][mU][mU][mC][mA][mU][mG][mA][mC][mU][mG][mU][mU][mA][mC][mU][mG][mA][mC][mC][mU]

Anti-miR-132: 5'-[mC][mG][mA][mC][mC][mA][mU][mG][mG][mC][mU][mG][mU][mA][mG][mA][mC][mU][mG][mU][mU][mA]-3'

For some experiments, the miRNAs and anti-miRNAs were obtained with a 5' Cy3 label. There was no appreciable difference between the control oligomers from Ambion or scrambled oligomers from Sigma in the assays (proliferation, tube formation and Matrigel) in which they were used as controls.

RNA extraction, reverse transcription PCR and miRNA profiling. RNA was extracted with the miRvana microRNA isolation kit (Ambion), and RT-PCR was performed with multiplexed TaqMan primers (Applied Biosystems). The miRNA profiles were generated with a 384-well microfluidic card-based TaqMan human microRNA panel (Applied Biosystems) amplified on a 7900

HT Fast Real Time PCR system (Applied Biosystems). Data were normalized to the internal control small RNA *RNU48*. Individual RT-PCRs were performed with TaqMan Assays (Applied Biosystems) on a SmartCycler (Cepheid) according to the manufacturers' instructions.

Proliferation assay. HUVECs were transfected with miRNAs or anti-miRNAs with siPORT-Neofx reagent (Ambion). BrdU was pulsed 48 h after transfection and cell proliferation was measured using an ELISA kit (Millipore). Ras activity was measured using a Ras Activity ELISA kit (Millipore) according to the manufacturer's instructions. An ELISA assay to measure phospho-MEK abundance was performed with a PathScan ELISA kit (Cell Signaling Technologies) according to the manufacturer's instructions.

Three-dimensional collagen tube formation assay. Tube formation assays were done as previously described³⁶. Briefly, 24 h after transfection of miRNAs or anti-miRNAs, HUVECs were seeded on a 3.75 mg ml⁻¹ type I collagen matrix (BD Biosciences) in a half-area 96-well plate (Sigma). Complete EBM-2 containing 10 μ g ml⁻¹ *Ulex europaeus* lectin (Vector Labs) was added 30 min later to enable live cell imaging. Tube lengths were measured and quantified with MetaMorph software (Molecular Devices).

MicroRNA *in situ* hybridization. The human hemangioma tissue array, human breast carcinoma tissue array and normal human tissue array were purchased from US Biomax. *In situ* hybridization was performed as previously described³⁷ with a digoxigenin-labeled miR-132 Locked Nucleic Acid (LNA) probe (probe sequence 5'-CGACCATGGCTGTAGACTGTTA-3'; Exiqon). Digoxigenin was detected by an digoxigenin-specific, horseradish peroxidase-labeled antibody (Roche) and amplified with a TSA-Plus Cy3 system (Perkin Elmer). miRNA expression was scored with Metamorph software (Molecular Devices).

Nanoparticle preparation. Liposomes incorporating an $\alpha_{v}\beta_3$ -targeting cyclic RGD peptide were prepared as previously described¹. Lipid-RNA complexes were formulated with a molar ratio of 4:1 calculated based on the *N*-[1-(2,3-dioleoyloxy)]-*N,N,N*-trimethylammonium propane (DOTAP) content of the liposomes. Nucleic acids (miRNAs or anti-miRNAs) and lipids were separately diluted in 100 μ l RNase-free water. The RNA solution was added to the liposomes, mixed gently and the mixture was incubated at 25 °C for 5 min before injection into mice.

***In vivo* assays.** Mouse experiments were performed under approval by the University of California–San Diego Institutional Animal Care and Use Committee. Typically, 6- to 8-week-old female mice (Jackson Labs) were used for all experiments. *Ert2*-ubiquitin-Cre mice were a gift from E. Brown (University of Pennsylvania), and *Rasa1*^{fl/fl} mice have been described elsewhere²⁰. Growth factor-reduced Matrigel (BD) containing either PBS or 400 ng ml⁻¹ recombinant human bFGF (Millipore) was injected subcutaneously into C57BL/6 mice. Mice were injected intravenously with 10 μ g control or anti-miRNAs. After 5 d, mice were injected with 10 μ g *Griffonia simplicifolia* lectin-FITC (Vector Labs), the plugs were collected and lysed in RIPA-buffer and the FITC content was measured on a spectrophotometer (Tecan). Retinal neovascularization studies were performed as previously described³⁸. Briefly, 5 μ g of control anti-miRNA or anti-miR-132 (both from Ambion) was injected into the vitreous cavity of 6-d-old neonatal BALB/c mice under light anesthesia. After 6 d, mice were killed and the retinas were dissected, fixed and stained with CD31-specific antibody. Mouse ID-8 VEGF ovarian carcinoma cells were a gift from G. Coukos (University of Pennsylvania) and have been previously described³⁹. Mice were implanted with Matrigel plugs containing 50,000 GFP⁺ ID8-VEGF cells and treated with intravenous injection of 10 μ g of scrambled anti-miRNA or anti-miR-132 (both from Sigma) in vascular targeted RGD-nanoparticles¹ 2, 4, 6 and 8 d after implantation. Plugs were collected and processed as described above.

MDA-MB-231 human breast carcinoma cells (2×10^6) were injected into the mammary fat pad (fat pad no. 4) of nude mice. Mice were treated with 50 μ g of scrambled anti-miRNA or anti-miR-132 (both from Sigma) in RGD-nanoparticles intravenously every 2 d starting from day 12 until the

end of the experiment. Injection of a single dose of anti-miR-132 in the RGD nanoparticles decreased tumor size transiently with a half-life of biological efficacy of 2 d (data not shown). Tumor volumes were calculated by the formula $V = (LW^2)/2$, where L and W denote the longer and shorter diameter, respectively.

For the orthotopic pancreatic tumor studies, 1×10^6 human pancreatic carcinoma cells were injected in 50 μ l saline into the tails of pancreases of 6- to 8-week-old male nude mice as previously described⁴⁰. The primary tumors were collected 6 weeks after injection and sectioned for immunofluorescent staining.

Immunofluorescence and microscopy. Imaging was performed on a Nikon Spectral C1 confocal microscope (Nikon C1si with EZC1 acquisition software, Nikon Instruments) with Plan Apo 10 \times /0.45 air, Plan Apo 20 \times /0.75 air and Plan Apo 60 \times /1.40 oil objective lenses (Nikon). All images were recorded with a sequential acquisition of the fluorescent channels to prevent fluorescence bleed-through. Images were analyzed with MetaMorph software (Molecular Devices) for determination of tube lengths, vessel density and colocalization. Image contrast and brightness parameters were adjusted across the whole image or equally across all the comparison groups when necessary. Staining intensity on immunohistochemistry slides was

quantified on an arbitrary scale (0 (no staining) to 4 (strong staining)) by observers blinded to the sample identity.

Statistical analyses. All statistical analyses were performed with Excel (Microsoft) or Prism (GraphPad). Two-tailed Student's t test or Mann-Whitney U test was used to calculate statistical significance. A P value < 0.05 was considered to be significant.

35. Munoz, R. *et al.* Highly efficacious nontoxic preclinical treatment for advanced metastatic breast cancer using combination oral UFT-cyclophosphamide metronomic chemotherapy. *Cancer Res.* **66**, 3386–3391 (2006).
36. Koh, W., Stratman, A.N., Sacharidou, A. & Davis, G.E. *In vitro* three dimensional collagen matrix models of endothelial lumen formation during vasculogenesis and angiogenesis. *Methods Enzymol.* **443**, 83–101 (2008).
37. Pena, J.T. *et al.* miRNA *in situ* hybridization in formaldehyde and EDC-fixed tissues. *Nat. Methods* **6**, 139–141 (2009).
38. Scheppke, L. *et al.* Retinal vascular permeability suppression by topical application of a novel VEGFR2/Src kinase inhibitor in mice and rabbits. *J. Clin. Invest.* **118**, 2337–2346 (2008).
39. Weis, S., Cui, J., Barnes, L. & Cheresh, D. Endothelial barrier disruption by VEGF-mediated Src activity potentiates tumor cell extravasation and metastasis. *J. Cell Biol.* **167**, 223–229 (2004).
40. Desgrosellier, J.S. *et al.* An integrin $\alpha_3\beta_3$ -c-Src oncogenic unit promotes anchorage-independence and tumor progression. *Nat. Med.* **15**, 1163–1169 (2009).